

# Effect of the Si/Al Ratios of Nanocrystalline HZSM-5 Zeolite on the Performance in Catalytic Conversion of Ethanol to Propylene

Tao Meng<sup>1</sup>, Dongsen Mao<sup>1,\*</sup>, Qiangsheng Guo<sup>1</sup>, and Zhen Ma<sup>2,\*</sup>

<sup>1</sup>Research Institute of Applied Catalysis, School of Chemical and Environmental Engineering, Shanghai Institute of Technology, Shanghai 201418, P. R. China

<sup>2</sup>Department of Environmental Science and Engineering, Fudan University, Shanghai 200433, P. R. China

Four ZSM-5 zeolite samples, with similar crystal sizes (about 100 nm) but different Si/Al molar ratios (nominal ratios from the compositions of the synthesis mixtures: 50, 75, 125, or 200; actual ratios determined by ICP: 50, 70, 131, 189), were synthesized hydrothermally and characterized by ICP-OES, SEM, XRD, N<sub>2</sub> adsorption–desorption, NH<sub>3</sub>-TPD, Py-IR, and TG. The characterization results showed that the structural and textural properties of these samples are identical to each other, but their acid properties are critically influenced by the Si/Al molar ratios. The amounts of Brønsted and Lewis acid sites increase when the Si/Al ratio decreases. The catalytic performance of these catalysts in the conversion of ethanol to propylene was examined in a fixed-bed micro-reactor at atmospheric pressure, 500 °C, and a WHSV of 1.58 h<sup>-1</sup>. HZSM-5 nanocatalysts with relatively low Si/Al ratios are favorable for the formation of propylene and butylene, whereas those with higher Si/Al ratios are favorable for the formation of ethylene. Possible reasons for the difference in selectivity of these catalysts are discussed.

**Keywords:** HZSM-5, Nanoscale, Si/Al Ratio, Ethanol, Propylene.

## 1. INTRODUCTION

Zeolites are crystalline aluminosilicates with ordered micropores and well-defined structures. In particular, ZSM-5 is useful in catalysis because it has abundant acid sites and excellent shape selectivity. ZSM-5-based catalysts have diversified functionalities, which makes them useful in the conversion of fossil fuels, the ablation of environmental pollutants, and the synthesis of fine chemicals.<sup>1–4</sup>

Conventional zeolites synthesized have crystal sizes on the order of micrometers. In recent years, nanoscale zeolites have attracted much interest because they may show better catalytic performance than conventional zeolites.<sup>5–7</sup> For example, nanosized ZSM-5 showed higher catalytic activity than micronsized ZSM-5 did in the transalkylation of benzene with 1,2,4-trimethylbenzene.<sup>5</sup> Nanosized H-ZSM-5 showed higher activity, stability, and propylene selectivity in the conversion of methanol to propylene, compared with microsized H-ZSM-5.<sup>6</sup> The activity

of a series of nanocrystalline ZSM-5 zeolites in the liquid phase acylation of anisole with acetic anhydride was found to increase with the decrease of ZSM-5's particle size.<sup>8</sup> Nanocrystalline Y and beta zeolites showed better performance in catalytic conversion of used palm oil for the production of biofuel than microcrystalline Y and beta zeolites did.<sup>7</sup>

Propylene, a useful chemical stock, is mainly produced as a byproduct in the catalytic cracking of naphtha and crude oil in petrochemical industry. However, these catalytic processes involve and generate a lot of environmentally unfriendly chemicals/materials/wastes. Considering the shortage of petroleum in the long run and the growing demand for propylene combined with environmental concerns, it would be desirable to seek alternative “cleaner” routes to propylene.

Ethanol can be widely and easily produced by the fermentation of renewable biomass feed-stocks such as corn, sugarcane, and cellulose. Bioethanol is used directly to fuel vehicles in Brazil, and it can be blended with gasoline to fuel vehicles in some countries such as the

\*Authors to whom correspondence should be addressed.

United States. Besides, ethanol, either from fermentation or chemical processes, can be used to produce chemicals such as propylene in a cleaner fashion.<sup>9–27</sup>

Ethanol can be converted to propylene over HZSM-5-based catalysts.<sup>10–20, 22–25, 27</sup> High propylene selectivity could be achieved when the reaction is conducted at a suitable temperature and a low weight hourly space velocity (WHSV),<sup>11, 13, 14</sup> or if HZSM-5 is modified with La,<sup>14, 15</sup> Zr,<sup>11</sup> Sr,<sup>13</sup> or P.<sup>12, 18–20, 25</sup> However, the propylene selectivity and reaction stability of HZSM-5 catalysts must be improved for their industrial applications.<sup>26</sup>

Recently, we tested the catalytic performance of a series of HZSM-5 zeolites with the same composition (Si/Al = 75) but with different crystal sizes (100, 250, 500 nm) in the conversion of ethanol to propylene.<sup>28</sup> HZSM-5 with the smallest size (100 nm) in that study showed the highest selectivities to propylene and butylene as well as the lowest selectivities to ethylene and aromatics. The selectivity to propylene on this catalyst was more stable on stream than those on HZSM-5 catalysts with bigger crystal sizes (250, 500 nm). The relatively stable generation of more propylene on nanosized HZSM-5 was ascribed to the zeolite's larger external surface area, more secondary pores, and shorter diffusion channels. Xia and co-workers also studied the influence of particle size of H-ZSM-5 on the catalytic conversion of ethanol to propylene, and found that smaller H-ZSM-5 is preferable for the formation of propylene.<sup>27</sup>

It is recognized that the acidity of HZSM-5 is another important factor that affects the propylene selectivity and reaction stability,<sup>11, 14, 18, 22, 29</sup> and the acidity of HZSM-5 depends greatly on the Si/Al ratio.<sup>11, 13–15, 29</sup> However, to the best of our knowledge, the influence of the Si/Al ratio of nanoscale HZSM-5 on the performance in ethanol to propylene process has not been reported. Xia et al. studied catalytic conversion of ethanol to propylene over micrometer-sized H-ZSM-5 samples with different Si/Al ratios, and found that the production distribution is independent of the Si/Al ratio.<sup>29</sup> In our current work, four nanoscale HZSM-5 samples with similar crystal sizes (100 nm) but different Si/Al ratios were synthesized, and the effect of Si/Al molar ratios on the catalytic performance for the selective conversion of ethanol to propylene was investigated and discussed.

## 2. EXPERIMENTAL DETAILS

### 2.1. Catalyst Preparation

All ZSM-5 samples were synthesized from clear gel solutions with molar composition of 36 TPAOH:1 Al<sub>2</sub>O<sub>3</sub>:2x SiO<sub>2</sub>:2300 H<sub>2</sub>O.<sup>28</sup> A required amount of aluminum isopropoxide (AIP) and deionized water were added to a 50 wt.% aqueous solution of tetrapropylammonium hydroxide (TPAOH). The mixture was stirred at 0 °C to obtain a clear solution. Tetraethylorthosilicate (TEOS) was added dropwise under stirring at room temperature. The solution

was stirred at room temperature overnight to ensure the complete hydrolysis of TEOS. The prepared mother gel was heated at 80 °C to remove alcohols and some water. The concentrated solution was crystallized in Teflon-lined stainless-steel autoclaves under autogenous pressure. The crystallization process was first carried out at 100 °C for 24 h and then at 170 °C for 30 h.

The solid product was recovered after several cycles of centrifuging and washing with deionized water, dried at 110 °C overnight, and calcined in air at 600 °C for 6 h. The obtained ZSM-5 samples were turned into the H-form by three consecutive ion exchanges in a large excess of 1 M solutions of NH<sub>4</sub>NO<sub>3</sub> at 90 °C, and calcined at 550 °C for 6 h. The obtained HZSM-5 samples are denoted as HZ-*x*, where *x* is the nominal Si/Al molar ratio (50, 75, 125, or 200).

### 2.2. Catalyst Characterization

X-ray diffraction (XRD) experiments were performed using a PANalytical X'Pert diffractometer operating with Ni  $\beta$ -filtered Cu K $\alpha$  radiation at 40 kV and 40 mA. Two theta angles ranged from 5° to 50° with a speed of 4° per minute.

SEM micrographs were obtained using a Hitachi S-4000 instrument. The bulk Si/Al molar ratios of the samples were determined by ICP-OES (PerkinElmer Optima 7000DV).

Nitrogen adsorption/desorption isotherms at –196 °C were obtained after outgassing the sample under vacuum at 200 °C for 12 h, using a Micromeritics ASAP2020 M+C adsorption apparatus.

Temperature programmed desorption of ammonia (NH<sub>3</sub>-TPD) was carried out on a conventional flow apparatus equipped with a thermal conductivity detector (TCD). A 0.1 g sample of 40–60 mesh was pretreated in flowing N<sub>2</sub> at 500 °C for 1 h, cooled to 100 °C, and then exposed to 10% NH<sub>3</sub>/N<sub>2</sub> (30 mL/min) for 1 h. The sample was purged with N<sub>2</sub> (30 mL/min) to remove physically adsorbed NH<sub>3</sub>. The measurements were conducted in flowing N<sub>2</sub> (30 mL/min) from 100 °C to 550 °C at a heating rate of 10 °C/min.

The Py-IR spectra were recorded using a Nicolet 6700 infrared spectrometer with a resolution of 4 cm<sup>-1</sup>. A self-supported 12 mm diameter circular wafer was placed in an infrared cell with CaF<sub>2</sub> windows and connected to a vacuum system. The wafer was dehydrated at 400 °C and at *P* < 10<sup>-4</sup> mbar for 150 min. After cooling to room temperature, pyridine vapors were adsorbed for 30 min. Finally, excess pyridine was desorbed by evacuation of the samples at the desired temperature for 30 min, and pyridine-adsorbed IR spectra were recorded.

Coke amount was determined by a thermogravimetric analyzer (Shimadzu DTG-60H), with spent sample in air from 30 °C to 850 °C at a heating rate of 10 °C/min. The weight loss between 400 °C and 700 °C in each profile was defined as the content of coke on the used catalyst.

### 2.3. Catalytic Testing

Catalytic reaction tests were conducted at 500 °C under atmospheric pressure in a continuous flow fixed-bed reactor made of stainless steel (inner diameter 6 mm). Prior to the catalytic testing, the fresh catalyst was activated at 500 °C for 1 h in N<sub>2</sub> flow. Ethanol (purity > 99.5%) was fed at the rate of 0.6 mL/h (controlled with a piston pump) through a 0.3 g catalyst (40–60 mesh) placed in the central zone of the reactor. The weight hourly space velocity (WHSV) of ethanol was 1.58 h<sup>-1</sup>. The effluent products were analyzed online via an Agilent 6820 gas chromatograph with a flame ionization detector (FID) and a HP-Plot-Q capillary column. The product lines were heated electrically to avoid unwanted condensation of the products.

## 3. RESULTS AND DISCUSSION

### 3.1. Structural and Textural Characterization

The Si/Al molar ratio of each HZSM-5 sample, as measured by ICP-OES (50, 70, 131, 189, Table I), is fairly similar to that of the clear gel solution (50, 75, 125, 200). For convenience, the HZSM-5 samples are denoted as HZ-*x*, where *x* is the nominal Si/Al molar ratio (50, 75, 125, or 200).

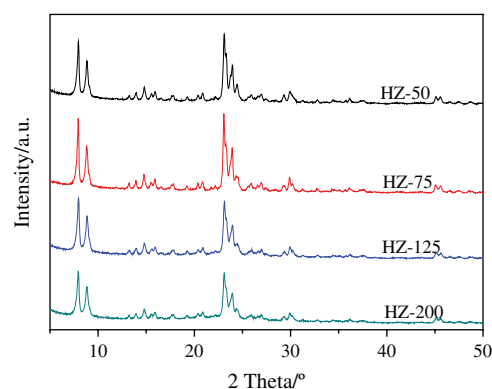
As shown in Figure 1, HZSM-5 samples with different Si/Al ratios exhibit the typical XRD patterns corresponding to the MFI-type structure, and no other peak can be observed. The very low background signal and sharp reflections indicate their excellent crystallinity.

Figure 2 shows the SEM micrographs of these samples. It can be seen that all the samples have almost the same spherical morphology, and their average particle sizes are all about 100 nm.

The results of N<sub>2</sub> adsorption and desorption measurements are summarized in Table I. Although the Si/Al ratios of HZSM-5 samples are different, there is only a marginal difference in the textural properties among these samples, probably owing to the similar crystal sizes of these samples.<sup>30</sup> The average pore diameters of these samples are large, due to the formation of many secondary pores by aggregation of nanoparticles.<sup>28</sup>

### 3.2. Acidity Characterization

NH<sub>3</sub>-TPD was performed to characterize the acidity of the catalysts. As shown in Figure 3, HZSM-5 catalysts



**Figure 1.** XRD patterns of HZSM-5 zeolites with different Si/Al ratios.

show typical NH<sub>3</sub>-TPD profiles with two maximum peaks below and above 300 °C, corresponding to NH<sub>3</sub> desorbed from weak and strong acid sites, respectively. The amounts of both weak and strong acid sites decrease as the Si/Al ratio of HZSM-5 increases, in agreement with previous studies.<sup>29–32</sup>

Figure 4 shows the IR spectra of pyridine adsorbed on HZSM-5 samples. The spectra of adsorbed pyridine exhibit characteristic bands at 1546 and 1448 cm<sup>-1</sup>, attributed to pyridinium ions (pyridine adsorbed on Brønsted (B) acid sites) and coordinatively bound pyridine (pyridine interacting with Lewis (L) acid sites), respectively. The signal at 1490 cm<sup>-1</sup> is assigned to pyridine on both B and L acid sites. The intensities of the bands at 1546, 1490, and 1448 cm<sup>-1</sup> all increase when the Si/Al ratio of HZSM-5 decreases, being the highest when the Si/Al ratio is 50.

The intensities of the bands at 1546 and 1448 cm<sup>-1</sup> were used to calculate the concentrations of B and L acid sites of HZSM-5 and the results are summarized in Table II. The values of B/L site ratios were calculated by the formula of 1.88A<sub>B</sub>/1.42A<sub>L</sub>, taking into account the coefficients of molar extinction.<sup>33</sup> The data show that the decrease in Si/Al ratio of HZSM-5 leads to a significant increase of the concentrations of both B and L acid sites at the same desorption temperature, consistent with the NH<sub>3</sub>-TPD results described above. On the other hand, the B/L ratio of HZSM-5 with different Si/Al ratios increases with the increase of pyridine desorption temperature, indicating that the B acid sites are stronger than the L acid sites.

**Table I.** Composition and textural properties of HZSM-5 zeolites with different Si/Al ratios.

Sample	Si/Al molar ratio <sup>a</sup>	BET surface area (m <sup>2</sup> · g <sup>-1</sup> )			Pore volume (cm <sup>3</sup> · g <sup>-1</sup> )			Average pore diameter (nm)
		Total	Micropore	External	Total	Micropore	Mesopore	
HZ-50	50.3	376	145	231	0.59	0.065	0.525	6.28
HZ-75	70.0	387	154	233	0.53	0.070	0.460	5.48
HZ-125	131.4	369	142	227	0.57	0.068	0.502	6.18
HZ-200	189.2	366	151	215	0.51	0.073	0.437	5.57

Note: <sup>a</sup>Determined by ICP-OES.

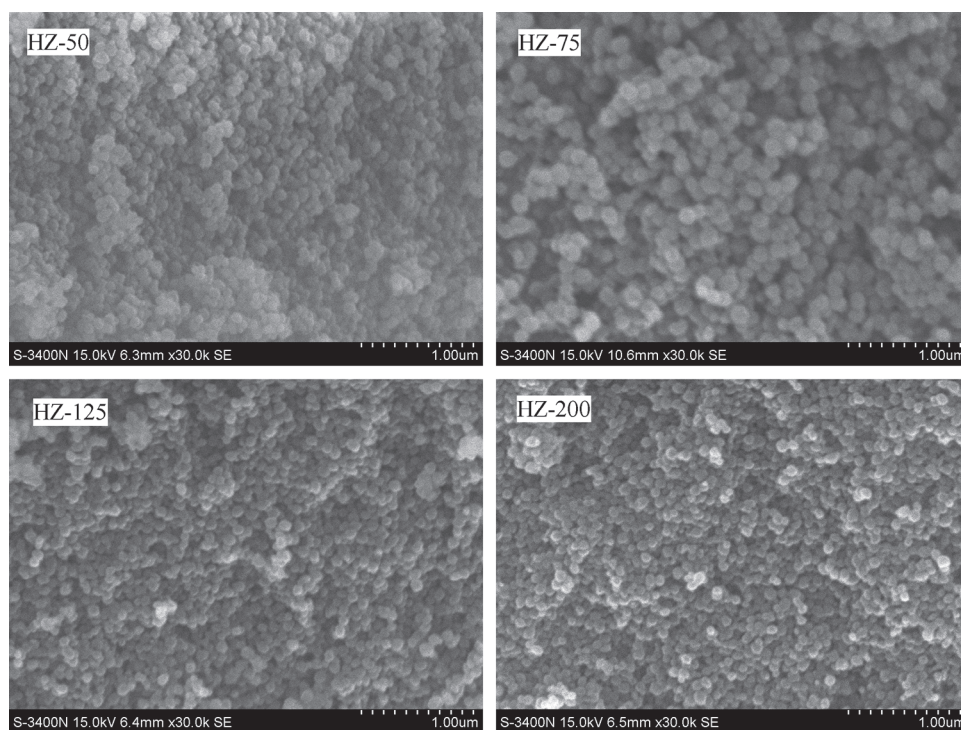


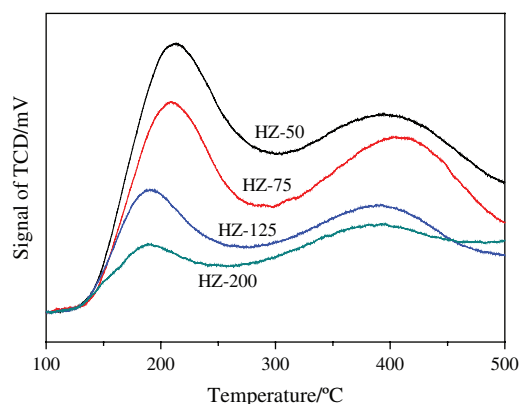
**Figure 2.** SEM images of HZSM-5 zeolites with different Si/Al ratios.

### 3.3. Catalytic Performance

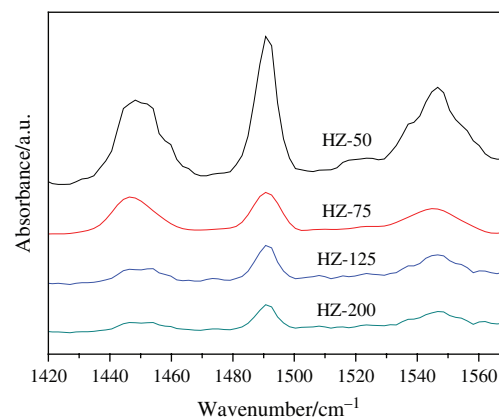
The catalytic performance of HZSM-5 catalysts with different Si/Al ratios in the conversion of ethanol into propylene (and other products such as ethylene, butylenes, and aromatics) was studied. For all the samples, the ethanol conversion is 100% during the whole operation. However, the initial selectivities to various products and their change patterns with respect to time on stream (TOS) are remarkably different for different catalysts.

Figure 5 shows the effects of TOS on the selectivities to light olefins ( $C_2$ – $C_4$ ) and aromatics. As presented in Figure 5(a), for HZ-50 with the lowest Si/Al ratio in this study, the propylene selectivity initially increases with TOS, reaching a maximum value (22.4%) at 30 h, and

then falls below 12% after 96 h on steam. A similar trend is observed for HZ-75; the highest propylene selectivity is 23.8% at 7.5 h, and the propylene selectivity falls below 12% after 54 h on stream. However, the propylene selectivities on HZ-125 and HZ-200 decrease rapidly with TOS. The selectivities to propylene on catalysts in the long run follow the sequence of HZ-50 > HZ-75 > HZ-125 > HZ-200. Apparently, HZ-50 is the most useful for the stable production of propylene. Previous investigations showed that a moderate surface acidity favors propylene production;<sup>11</sup> here we found that nanoscale HZ-50 with the largest amount of acid sites among the catalysts studied here is the best for propylene production. Our result



**Figure 3.**  $NH_3$ -TPD curves of HZSM-5 zeolites with different Si/Al ratios.



**Figure 4.** IR spectra of pyridine adsorbed on the different HZSM-5 zeolites after desorption at 100 °C.

**Table II.** Results of IR spectra of Py adsorbed on the different HZSM-5 zeolites after desorption at different temperatures.

Sample	100 °C		300 °C		B/L <sup>c</sup>	
	A <sub>B</sub> <sup>a</sup>	A <sub>L</sub> <sup>b</sup>	A <sub>B</sub>	A <sub>L</sub>	100 °C	300 °C
HZ-50	1.41	1.42	0.76	0.46	1.32	2.19
HZ-75	0.41	0.61	0.32	0.10	0.89	4.24
HZ-125	0.31	0.26	0.22	0.09	1.58	3.24
HZ-200	0.20	0.17	0.13	0.08	1.56	2.15

Note: <sup>a</sup>A<sub>B</sub>—Integrated area of peak at 1546 cm<sup>-1</sup>; <sup>b</sup>A<sub>L</sub>—Integrated area of peak at 1448 cm<sup>-1</sup>; <sup>c</sup>B/L—Calculated by the formula of 1.88A<sub>B</sub>/1.42A<sub>L</sub>.

is different from Goto et al.'s finding that HZSM-5 with a SiO<sub>2</sub>/Al<sub>2</sub>O<sub>3</sub> ratio of 184 is better than HZSM-5 with a SiO<sub>2</sub>/Al<sub>2</sub>O<sub>3</sub> ratio of 52 in terms of propylene production.<sup>13</sup>

The variation trend of butylene selectivity of each HZSM-5 sample is similar to propylene selectivity (Fig. 5(b)), implying that propylene and butylene might be produced through parallel pathways and common intermediate on the catalyst.<sup>20,34</sup> In addition, the selectivities to butylene on catalysts in the long run follow the sequence of HZ-50 > HZ-75 > HZ-125 > HZ-200.

As presented in Figure 5(c), the selectivities to ethylene on HZSM-5 catalysts follow the sequence of HZ-50 < HZ-75 < HZ-125 < HZ-200, and they all increase with TOS. On the other hand, the selectivities to aromatics on

HZSM-5 catalysts follow the sequence of HZ-50 > HZ-75 > HZ-125 > HZ-200, and they all decrease with TOS (Fig. 5(d)). Song et al.<sup>11</sup> and Inoue et al.<sup>16</sup> found that lower surface acidity leads to the formation of more ethylene, while aromatics are promoted at higher acidity. Indeed, here we found that HZ-200 with the lowest surface acidity is more favorable for the formation of ethylene than HZ-125, HZ-75, and HZ-50, whereas HZ-50 with the highest acidity is more favorable for the formation of aromatics than HZ-75, HZ-125, and HZ-200. In addition, the changes of the selectivities of ethylene and aromatics with TOS in Figures 5(c and d) can be explained by the deactivation of the strong acidic sites due to the coke deposition.<sup>28</sup>

### 3.4. Correlation Between Acidity and Catalytic Performance

The reaction pathway of ethanol to propylene over HZSM-5 can be assumed as follows.<sup>14,35</sup> Ethanol is first converted to ethylene on acid sites. Higher hydrocarbons such as propylene are produced from ethylene via oligomerization-cracking. These conversions proceed over different acid sites: ethanol dehydration to ethylene can occur on weak acid sites, but the subsequent reaction steps require stronger acid sites.<sup>34,36</sup> Generally, the catalyst with high acid density and strong acidity convert intermediate hydrocarbons such as ethylene into higher

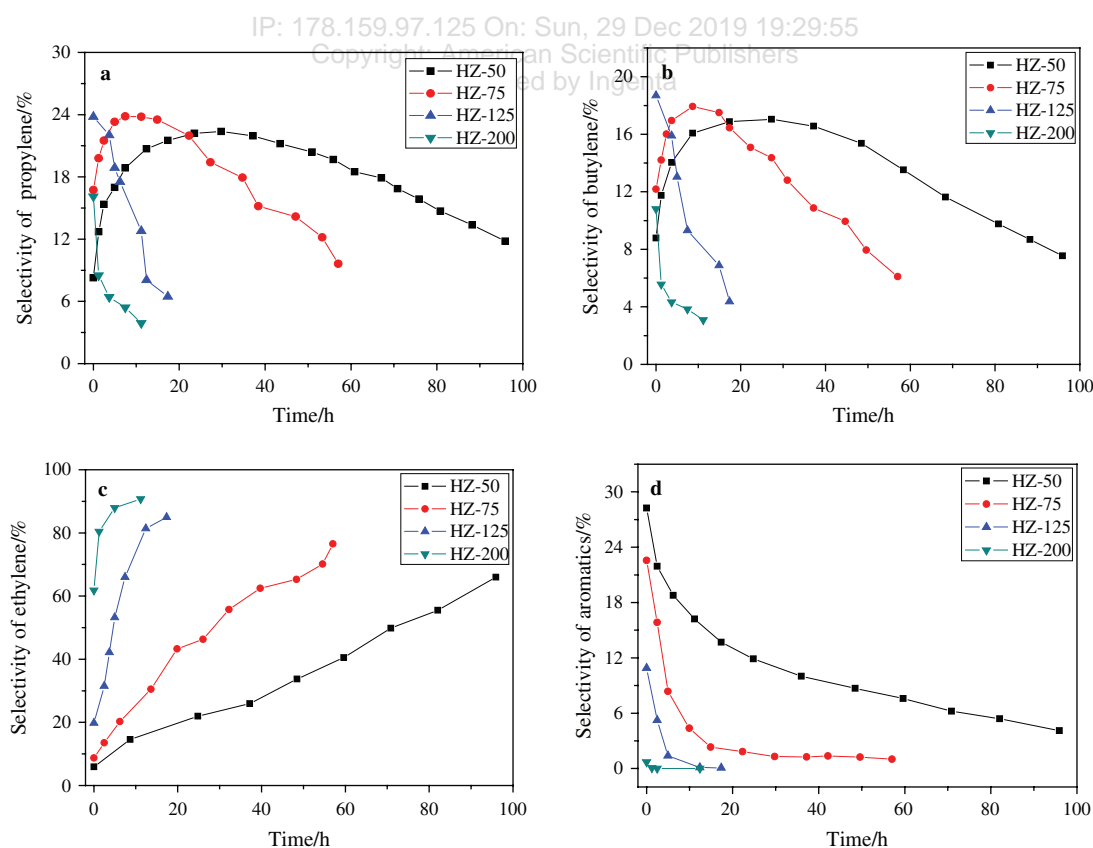


**Figure 5.** Effect of time on stream on selectivity of C<sub>2</sub>–C<sub>4</sub> olefins and aromatics over HZSM-5 zeolites with different Si/Al ratios at atmospheric pressure, 500 °C and WHSV = 1.58 h<sup>-1</sup>: (a) propylene; (b) butylene; (c) ethylene; (d) aromatics.

hydrocarbons ( $C_{3+}$  aliphatic and aromatic) species and coke.<sup>35</sup>

For fresh HZSM-5 with lower Si/Al ratios and larger amounts of strong acid sites, more aromatics are expected to be produced by aromatization.<sup>11,16</sup> Thus, HZ-50 and HZ-75 exhibit high initial aromatics selectivity (Fig. 5(d)) and low initial  $C_3$ – $C_4$  olefins selectivity (Figs. 5(a and b)). On the other hand, initial ethylene selectivity increases with the Si/Al ratio (Fig. 5(c)), indicating that weaker acid sites are beneficial for the formation of ethylene.

The catalyst surface is covered by coke gradually with TOS, thus inducing the decrease in the number of strong acid sites. Therefore, the selectivities of  $C_2$ – $C_4$  olefins increase but the selectivity to aromatics decreases with TOS. It can be concluded that decreasing the amount of strong acid sites is beneficial for raising propylene selectivity.<sup>22</sup> As the reaction over HZSM-5 prolongs, more and more coke is formed and covers the catalyst surface. Accordingly, the number of acid sites with medium strength, responsible for the formation of propylene and butylenes,<sup>11,16,22</sup> also decreases with TOS. As a result, the selectivity to  $C_3$ – $C_4$  olefins decreases, whereas ethylene selectivity keeps increasing.

The Si/Al ratio of HZSM-5 plays an important role in the time length of the induction period. HZSM-5 samples of low Si/Al ratios (50, 75) have larger numbers of strong acid sites, so more coke is needed to cover the strong acid sites, which makes the induction period longer. On the contrary, the numbers of strong acid sites on HZSM-5 samples with high Si/Al ratios (125, 200) are fewer, so these strong acid sites can be covered readily by smaller amounts of coke. Therefore, the induction period is much shorter for high Si/Al ratio samples. For the same reason, the order of the reduction rate of propylene selectivity over different HZSM-5 catalysts (HZ-200 > HZ-125 > HZ-75 > HZ-50) is opposite to that of the time length of the induction period. Our data indicate that high Si/Al ratio HZSM-5 zeolites are not suitable for catalytic reaction of ethanol to propylene, which is different from the trend seen in the methanol to propylene process.<sup>37</sup>

The above discussion suggests that the catalytic properties of HZSM-5 catalysts can be greatly affected by coke deposition. Additionally, since the samples are black in color after the reaction, coke deposition might be the main reason for catalyst deactivation.<sup>20,38</sup> TG was used to reveal the contents of coke over the spent catalysts. Figure 6 shows that, the relative amount of carbonaceous deposits for the used HZ-50 collected after 96 h on stream is 8.50%, that for the used HZ-75 collected after 57 h on stream is 3.50%, that for the used HZ-125 collected after 17 h on stream is 0.64%, and that for the used HZ-200 collected after 11 h on stream is 0.40%. With more coke deposits on it, HZ-50 still has higher propylene selectivity than the other catalysts (Fig. 5(a)), indicating that HZ-50 has better ability to tolerate the coke deposits.

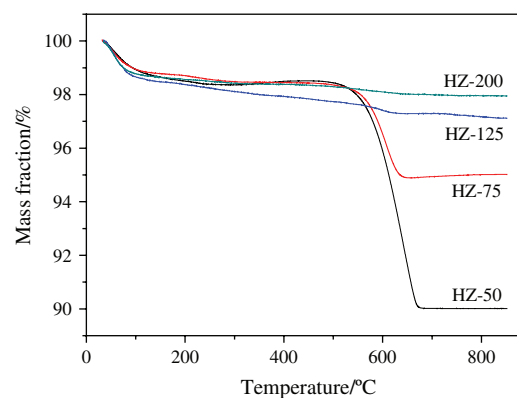


**Figure 6.** TG curves of HZSM-5 zeolites with different Si/Al ratios after the duration test of ethanol to propylene catalytic reaction.

#### 4. CONCLUSIONS

ZSM-5 zeolites with different Si/Al ratios (50, 75, 115, 200) but similar crystal sizes (100 nm) were successfully synthesized. These HZSM-5 catalysts had similar physicochemical properties except for the acidity. The decreased Si/Al molar ratio of ZSM-5 zeolite led to an increase in the amounts of the strong acid sites and weak acid sites. HZSM-5 with different Si/Al molar ratios all exhibited high activity for ethanol conversion. In particular, HZSM-5 with a Si/Al ratio of 50 was found to be the most favorable for the stable production of propylene. Further attempts may be made to modify the catalyst in order to improve the propylene yield and stability.

**Acknowledgment:** The authors thank Shanghai Municipal Education Commission (J51503) and Graduate Innovation Foundation of Shanghai Institute of Technology (yjscx2010005) for financial support.

#### References and Notes

1. F. Kapteijn, J. Rodriguez-Mirasol, and J. A. Moulijn, *Appl. Catal. B* 9, 25 (1996).
2. N. Rahimi and R. Karimzadeh, *Appl. Catal. A* 398, 1 (2011).
3. B. Kaur and R. Srivastava, *J. Nanosci. Nanotechnol.* 14, 6539 (2014).
4. L. T. Hoai Nam, T. Q. Vinh, N. T. Thanh Loan, N. T. Nhiem, N. T. Thu Trang, N. M. Tan, and J. Radnik, *J. Nanosci. Nanotechnol.* 15, 7275 (2015).
5. X. J. Cheng, X. S. Wang, and H. Y. Long, *Micropor. Mesopor. Mater.* 119, 171 (2009).
6. M. Firoozi, M. Baghalha, and M. Asadi, *Catal. Commun.* 10, 1582 (2009).
7. N. Taufiqurrahmi, A. R. Mohamed, and S. Bhatia, *J. Nanopart. Res.* 13, 3177 (2011).
8. R. Selvin, H. L. Hsu, and T. M. Her, *Catal. Commun.* 10, 169 (2008).
9. J. Rass-Hansen, H. Falsig, B. Jørgensen, and C. H. Christensen, *J. Chem. Technol. Biotechnol.* 82, 329 (2007).
10. K. Murata, M. Inaba, and I. Takahara, *J. Jap. Petro. Inst.* 51, 234 (2008).
11. Z. X. Song, A. Takahashi, N. Mimura, and T. Fujitani, *Catal. Lett.* 131, 364 (2009).
12. Z. X. Song, A. Takahashi, I. Nakamura, and T. Fujitani, *Appl. Catal. A* 384, 201 (2010).

13. D. Goto, Y. Harada, Y. Furumoto, A. Takahashi, T. Fujitani, Y. Oumi, M. Sadakane, and T. Sano, *Appl. Catal. A* 383, 89 (2010).
14. K. Inoue, M. Inaba, I. Takahara, and K. Murata, *Catal. Lett.* 136, 14 (2010).
15. K. Inoue, K. Okabe, M. Inaba, I. Takahara, and K. Murata, *React. Kinet. Mech. Catal.* 101, 477 (2010).
16. K. Inoue, K. Okabe, M. Inaba, I. Takahara, and K. Murata, *React. Kinet. Mech. Catal.* 101, 227 (2010).
17. C. Duan, X. Zhang, R. Zhou, Y. Hua, J. Chen, and L. Zhang, *Catal. Lett.* 141, 1821 (2011).
18. Y. Furumoto, Y. Harada, N. Tsunoji, A. Takahashi, T. Fujitani, Y. Ide, M. Sadakane, and T. Sano, *Appl. Catal. A* 399, 262 (2011).
19. Y. Furumoto, N. Tsunoji, Y. Ide, M. Sadakane, and T. Sano, *Appl. Catal. A* 417–418, 137 (2012).
20. A. Takahashi, W. Xia, I. Nakamura, H. Shimada, and T. Fujitani, *Appl. Catal. A* 423–424, 162 (2012).
21. M. Iwamoto, S. Mizuno, and M. Tanaka, *Chem.-Eur. J.* 19, 7214 (2013).
22. Z. X. Song, W. Liu, C. Chen, A. Takahashi, and T. Fujitani, *React. Kinet. Mech. Catal.* 109, 221 (2013).
23. C. Duan, X. Zhang, R. Zhou, Y. Hua, L. Zhang, and J. Chen, *Fuel Process. Technol.* 108, 31 (2013).
24. Y. Takamitsu, K. Yamamoto, S. Yoshida, H. Ogawa, and T. Sano, *J. Porous Mater.* 21, 433 (2014).
25. N. Tsunoji, T. Sonoda, Y. Furumoto, M. Sadakane, and T. Sano, *Appl. Catal. A* 481, 161 (2014).
26. M. Iwamoto, *Catal. Today* 242, Part B, 243 (2015).
27. W. Xia, K. Chen, A. Takahashi, X. Y. Li, X. C. Mu, C. Han, L. Liu, I. Nakamura, and T. Fujitani, *Catal. Commun.* 73, 27 (2016).
28. T. Meng, D. S. Mao, Q. S. Guo, and G. Z. Lu, *Catal. Commun.* 21, 52 (2012).
29. W. Xia, A. Takahashi, I. Nakamura, H. Shimada, and T. Fujitani, *J. Mol. Catal. A* 328, 114 (2010).
30. A. S. Al-Dughaiter and H. de Lasa, *Ind. Eng. Chem. Res.* 53, 15303 (2014).
31. P. L. Benito, A. G. Gayubo, A. T. Aguayo, M. Olazar, and J. Bilbao, *J. Chem. Technol. Biotechnol.* 66, 183 (1996).
32. A. G. Gayubo, P. L. Benito, A. T. Aguayo, M. Olazar, and J. Bilbao, *J. Chem. Technol. Biotechnol.* 65, 186 (1996).
33. C. A. Emeis, *J. Catal.* 141, 347 (1993).
34. A. T. Aguayo, A. G. Gayubo, A. M. Tarrío, A. Atutxa, and J. Bilbao, *J. Chem. Technol. Biotechnol.* 77, 211 (2002).
35. N. R. C. F. Machado, V. Calsavara, N. G. C. Astrath, C. K. Matsuda, A. Paesano Junior, and M. L. Baesso, *Fuel* 84, 2064 (2005).
36. F. F. Madeira, N. S. Gnep, P. Magnoux, H. Vezin, S. Maury, and N. Cadran, *Chem. Eng. J.* 161, 403 (2010).
37. M. Inaba, K. Murata, I. Takahara, and K.-I. Inoue, *J. Chem. Technol. Biotechnol.* 86, 95 (2011).
38. N. R. C. Fernandes Machado, V. Calsavara, N. G. C. Astrath, A. M. Neto, and M. L. Baesso, *Appl. Catal. A* 311, 193 (2006).

Received: 11 April 2016. Accepted: 8 May 2016.

IP: 178.159.97.125 On: Sun, 29 Dec 2019 19:29:55  
Copyright: American Scientific Publishers  
Delivered by Ingenta